

Voltage-Gated Na Channels

ω-Grammotoxin-SIA inhibits voltage-gated Na⁺ channel currents

Rita de Cássia Collaço¹, Filip Van Petegem^{2,3}, and Frank Bosmans^{1,4}

ω-Grammotoxin-SIA (GrTX-SIA) was originally isolated from the venom of the Chilean rose tarantula and demonstrated to function as a gating modifier of voltage-gated Ca²⁺ (Ca_V) channels. Later experiments revealed that GrTX-SIA could also inhibit voltage-gated K⁺ (K_V) channel currents via a similar mechanism of action that involved binding to a conserved S3–S4 region in the voltage-sensing domains (VSDs). Since voltage-gated Na⁺ (Na_V) channels contain homologous structural motifs, we hypothesized that GrTX-SIA could inhibit members of this ion channel family as well. Here, we show that GrTX-SIA can indeed impede the gating process of multiple Na_V channel subtypes with Na_V1.6 being the most susceptible target. Moreover, molecular docking of GrTX-SIA onto Na_V1.6, supported by a p.E1607K mutation, revealed the voltage sensor in domain IV (VSDIV) as being a primary site of action. The biphasic manner in which current inhibition appeared to occur suggested a second, possibly lower-sensitivity binding locus, which was identified as VSDII by using K_V2.1/Na_V1.6 chimeric voltage-sensor constructs. Subsequently, the Na_V1.6^{p.E782K/p.E838K} (VSDII), Na_V1.6^{p.E1607K} (VSDIV), and particularly the combined VSDII/VSDIV mutant lost virtually all susceptibility to GrTX-SIA. Together with existing literature, our data suggest that GrTX-SIA recognizes modules in Na_V channel VSDs that are conserved among ion channel families, thereby allowing it to act as a comprehensive ion channel gating modifier peptide.

Introduction

ω-Grammotoxin-SIA (GrTX-SIA) is a 36-amino acid peptide isolated from the venom of the Chilean rose tarantula (Grammostola rosea, G. spatulata, or G. cala) (Lampe et al., 1993) and is organized according to the ubiquitous inhibitory cystine-knot scaffold (Pallaghy et al., 1994; Takeuchi et al., 2002; Norton and McDonough, 2008; Dongol et al., 2019). As such, GrTX-SIA belongs to a large group of structurally related venom peptides that have been documented to target members of one or more ion channel families (Kalia et al., 2015). Notably, GrTX-SIA was originally identified as an inhibitor of P/Q- and N-type voltagegated Ca²⁺ (Ca_V) channels because of its modulatory effects on voltage-dependent gating (Lampe et al., 1993; McDonough et al., 1997). Indeed, when tested on a range of animal tissues, GrTX-SIA prevented: (1) depolarization-induced Ca²⁺ influx into brain synaptosomes (Lampe et al., 1993), (2) electrically evoked Ca²⁺ influx in dorsal root ganglion neurons (Piser et al., 1994), (3) norepinephrine or aspartate release from brain slices (Keith

et al., 1995), and (4) glutamate release from cultured brain synaptosomes and hippocampal neurons (Piser et al., 1995a, 1995b). Correspondingly, perfusion of GrTX-SIA into rat hippocampus led to a concentration-dependent reduction in glutamate and serotonin release with higher concentrations inducing convulsive-like behavior (Keith et al., 1995). In contrast to P/Q-and N-type, L-type Ca_V channels were reported to be insensitive to GrTX-SIA (Lampe et al., 1993; Piser et al., 1994).

About 5 years after its discovery, the amino acid sequence homology between GrTX-SIA and hanatoxin (Swartz and MacKinnon, 1995) as well as their similar mechanism of action, albeit on different ion channel families, prompted experiments in which GrTX-SIA was found to inhibit voltage-gated K^+ (K_V) channels as well (Li-Smerin and Swartz, 1998). Moreover, this study also indicated that hanatoxin and GrTX-SIA could likely interact with similar regions in both Ca_V and K_V channel voltage-sensing domains (VSDs) to modify their gating process.

¹Department of Basic and Applied Medical Sciences, Molecular Physiology and Neurophysics Group, Ghent University, Ghent, Belgium; ²Department of Biochemistry and Molecular Biology, University of British Columbia, Vancouver, Canada; ³Life Sciences Institute, University of British Columbia, Vancouver, Canada; ⁴Faculty of Medicine and Pharmacy, Center for Neurosciences (C4N), Vrije Universiteit Brussel, Brussels, Belgium.

Correspondence to Frank Bosmans: frank.bosmans@ugent.be

This work is part of a special issue on Voltage-Gated Sodium (Na_v) Channels.

© 2024 COLLAÇO et al. This article is distributed under the terms of an Attribution–Noncommercial–Share Alike–No Mirror Sites license for the first six months after the publication date (see http://www.rupress.org/terms/). After six months it is available under a Creative Commons License (Attribution–Noncommercial–Share Alike 4.0 International license, as described at https://creativecommons.org/licenses/by-nc-sa/4.0/).





During the following years, it became clear that these structural motifs are composed of the S3 and S4 transmembrane helices (Swartz and MacKinnon, 1997), and that they are virtually conserved in Ca_V and K_V channels (Bourinet et al., 2001; Jiang et al., 2003; Swartz, 2008; Bosmans and Swartz, 2010; Catterall, 2011; Bladen et al., 2014; Kuang et al., 2015; Van Theemsche et al., 2020; Yao et al., 2024). Notably, the architecture of VSDs in voltage-gated Na⁺ (Na_V) channels resemble those of Ca_V and K_V channels, suggesting possible interaction sites for these peptides (Jiang et al., 2003; Swartz, 2008; Chakrapani et al., 2008; Ahern et al., 2016; Clairfeuille et al., 2019; Catterall et al., 2020; Noreng et al., 2021; Li et al., 2024; Ngo et al., 2024). Indeed, hanatoxin and related K_V channel toxins can potently affect Na_V channel gating in a manner that is dependent on which VSD is primarily targeted and how this sensor is coupled to various aspects of Na_V channel gating (Bosmans et al., 2008, 2011; Bosmans and Swartz, 2010; Ahern et al., 2016). For example, toxins that target the voltage-sensing region in domains I-III (VSDI-III) influence opening of the channel, whereas toxins typically need to interact specifically with the voltage sensor in domain IV (VSDIV) to impede inactivation (Hodgkin and Huxley, 1952; Sheets et al., 1999; Chanda and Bezanilla, 2002; Chanda et al., 2004; Campos et al., 2008; Ahern et al., 2016).

Based on these observations of promiscuous toxin behavior, we postulated that GrTX-SIA could also bind to one or more $\rm Na_V$ channel VSDs to influence gating. To test our hypothesis, we expressed eight $\rm Na_V$ channel subtypes ($\rm Na_V1.1-Na_V1.8$) in Xenopus laevis oocytes and measured toxin-induced effects using the two-electrode voltage-clamp technique. To outline a potential working mechanism, we combined molecular docking of GrTX-SIA onto $\rm Na_V1.6$, the most susceptible subtype, with point mutagenesis and the use of $\rm K_V2.1/Na_V1.6$ chimeric S3–S4 voltage-sensor constructs.

Materials and methods

Toxins and reagents

Lyophilized GrTX-SIA (CAS No.: 152617-90-8) and tetrodotoxin (CAS No.: 18660-81-6) were purchased from Alomone Labs and TOCRIS, respectively. Both toxins were dissolved in a recording solution supplemented with 0.1% BSA (bovine serum albumin, CAS No.: 9048-46-8) and stored at -20°C before use. Analytical grade reagents, enzymes, and antibiotics used in solutions were purchased from Sigma-Aldrich/Merck.

Xenopus oocyte protein expression

The cDNA sequences of $Na_V1.1$ (AF225985), $Na_V1.2$ (NP001035232), $Na_V1.3$ (AF225987), $Na_V1.4$ (NP000325), $Na_V1.5$ (AAI44622), $Na_V1.6$ (NP055006), $Na_V1.7$ (NP002968), $Na_V1.8$ (NP058943), and $\beta1$ (NP001028) were obtained from Origene and Genscript and confirmed by automated Sanger sequencing. The chimeric $K_V2.1/Na_V1.6$ constructs were previously described (Montnach et al., 2022). Mutations in human $Na_V1.6$ were inserted and verified by Genscript. Plasmids were linearized with an applicable restriction enzyme and RNA transcriptions were performed using the T7 polymerase or SP6 (for $Na_V1.8$) polymerases (mMessage mMachine kit; Life Technologies). The

resulting cRNA of all constructs was dissolved in RNAse-free water and stored at -80°C prior to use. *Xenopus* frogs, obtained from Nasco and kept at the Department of Biomedical Molecular Biology (UGent), were handled in accordance with the UGent University Animal Care and Use Committee (protocol No.: ECD 23-02), Guide for the Care and Use of Laboratory Animals and the European Directive 86/609/EEC.

Na $_{\rm V}$ channels were expressed with $\beta 1$ by microinjecting RNA in a 1:5 M ratio into defolliculated *Xenopus* oocytes as previously reported (Bosmans et al., 2008). The injected volume per oocyte was 50 nl with the following ion channel RNA concentrations: Na $_{\rm V}1.1500$ ng/ μ l, Na $_{\rm V}1.2200$ ng/ μ l, Na $_{\rm V}1.3200$ ng/ μ l, Na $_{\rm V}1.41,000$ ng/ μ l, Na $_{\rm V}1.5100$ ng/ μ l, Na $_{\rm V}1.6$ wild-type/mutants 500 ng/ μ l, Na $_{\rm V}1.71,000$ ng/ μ l, Na $_{\rm V}1.81,000$ ng/ μ l, and the K $_{\rm V}2.1/{\rm Na}_{\rm V}1.6$ chimeras 200 ng/ μ l. After injection and before use, oocytes were incubated for 1–3 days at 17°C in Barth's medium (in mM: 96 NaCl, 2 KCl, 5 HEPES (2-[4-(2-hydroxyethyl) piperazin-1-yl]methanesulfonic acid), 1 MgCl $_{\rm 2}$, 1.8 CaCl $_{\rm 2}$, and 50 μ g/ml gentamycin, pH 7.6 with NaOH).

Two-electrode voltage-clamp technique

Following incubation, ionic currents were studied using the two-electrode voltage-clamp recording technique (model OC-725C; Warner Instruments) with a 150-µl recording chamber as previously described (Bosmans et al., 2008). Briefly, this established approach enables control of the transmembrane potential of cells and precise measurement of the ion flow across the cell membrane through voltage-gated ion channels as an electric current. Thus, it becomes possible to examine biophysical gating parameters (i.e., opening/closing) of voltage-gated ion channels in response to changes in the transmembrane potential and investigate the influence of GrTX-SIA on channel function. All data were filtered at 4 kHz (tunable active filter model nine hundred; Frequency Devices Inc.) and digitized at 20 kHz using pClamp 10 software (Molecular Devices). For Na_V channels, the external recording solution used was ND-100 (in mM: 100 NaCl, 5 HEPES, 1 MgCl $_2$, and 1.8 CaCl $_2$, pH 7.6 with NaOH). For K_V channel measurements, a 50K solution (in mM: 50 KCl, 50 NaCl, 0.3 CaCl₂, 1 MgCl₂, and 5 HEPES, pH 7.6 with NaOH) was used. Borosilicate microelectrode resistances (produced with a Narishige PC-10 vertical puller) were 0.5–1.0 $M\Omega$ when backfilled with 3 M KCl. All experiments were performed at room temperature (\sim 22°C).



(flow rate \sim 1 ml/min) with ND-100 or 50K. Linear components of capacity and leak currents were identified and subtracted by inhibiting channels with 1 μ M tetrodotoxin.

Molecular modeling

To find possible residues involved in GrTX-SIA binding to $Na_V1.6$, we used AlphaFold (version 2.3; DeepMind) (Jumper et al., 2021) to predict structures of GrTX-SIA in complex with either full-length human $Na_V1.6$ or the individual VSDII or IV. For each run, the top hits were further energy-minimized to remove potential geometrical errors. These predictions were performed using computational resources from the Digital Research Alliance of Canada. Predicted structures and their associated predicted local distance difference test (pLDDT) scores were analyzed using PyMol (Schrodinger), whereas positional alignment error (PAE). Scores were evaluated in ChimeraX (University of California, San Francisco) (Meng et al., 2023). Figures of the predicted complexes were made using PyMol (Schrodinger).

Data and statistical analysis

Electrophysiological data were analyzed offline with Clampfit 11.1 (Molecular Devices) and Prism 8 (GraphPad). Conductance (G) was calculated as in Eq. 1. For normalization to pretoxin conditions, conductance and current (I) measurements after GrTX-SIA incubation were divided by the respective $G_{\rm max}$ or $I_{\rm max}$ of that particular oocyte. Normalized $G/G_{\rm max}$ and $I/I_{\rm max}$ relationships were fitted to Eq. 2.

$$G = I/(Va - Ve), (1$$

in which I: current at an applied voltage, Va: applied voltage (mV), Ve: equilibrium potential (mV)

$$G/G_{max}$$
(or I/I_{max}) = $\{1 + exp[-zF(V - V_{1/2})/RT]\}^{-1}$ (2)

in which, z: equivalent charge, F: Faraday's constant, V: voltage, $V_{1/2}$: half-activation voltage, R: gas constant, and T: temperature in Kelvin.

Voltage-dependence of slow inactivation was measured after a 10 s-pulse at multiple voltages followed by a depolarizing pulse to peak current voltage, which was normalized to maximum amplitude ($I_{\rm max}$), and plotted versus conditioning potential. Recovery from fast inactivation was obtained by applying two depolarizing pulses with varying lengths of time in between to the voltage of peak current for each channel subtype; the second pulse was divided by the first pulse at that time point for normalization purposes. Single-exponential time constants (τ), which correspond to 64% decay (1/e) of the peak current, were calculated and indicated.

Between two sets of data, statistically significant differences (P < 0.05) were assessed using two-tailed Student's t tests. To compare one time point between more than two groups, oneway ANOVA followed by Tukey's post hoc analysis was used (P < 0.05). To compare multiple time points between two groups, two-way ANOVA followed by Bonferroni's post hoc analysis was adopted (P < 0.05). Data are presented as mean \pm SEM of n independent oocytes, as stated in the Results section.

Online supplemental material

Fig. S1 shows the electrophysiology protocols used and $Na_V1.6$ inactivation. Fig. S2 shows GrTX-SIA and $Na_V1.6$ slow inactivation. Fig. S3 shows GrTX-SIA interacts with VSDII and VSDIV in $Na_V1.6$. Table S1 shows the influence of GrTX-SIA on the gating properties of $Na_V1.1-1.8$. Table S2 shows concentration-response data. Table S3 shows the influence of GrTX-SIA on the gating properties of $Na_V1.6$ mutants.

Results

GrTX-SIA inhibits Nav channel currents

We initially determined Na_V channel sensitivity for GrTX-SIA by applying 100 nM toxin to oocytes expressing Na_V1.1-Na_V1.8 and assessing conductance-voltage (G-V) and channel availability relationships. At 100 nM, GrTX-SIA significantly (P < 0.05) reduced currents of all tested Na_V channel subtypes, albeit to a varying degree (Fig. 1 and Table S1). Na_v1.8 and Na_v1.2 were least inhibited (12 \pm 4% and 19 \pm 5%, respectively), followed by $Na_V 1.3 (23 \pm 9\%)$, $Na_V 1.5 (27 \pm 10\%)$, $Na_V 1.7 (31 \pm 6\%)$, $Na_V 1.4 (32 \pm 10\%)$ 13%), and Na_V1.1 (54 \pm 5%). The most substantial current reduction was observed with Na_V1.6 (57 ± 9%). Window currents were reduced by 6% (Na_V1.8), 22% (Na_V1.2), 34% (Na_V1.3), 39% (Na_V1.5), 4% (Na_V1.7), 29% (Na_V1.4), 65% (Na_V1.1), and 38% (Na_V1.6). At 100 nM, the $V_{1/2}$ deduced by a fit of the G-V relationship to Eq. 2 was significantly shifted to depolarized voltages for $Na_V1.1$ (~3 mV), $Na_V1.2$ (~2 mV), $Na_V1.3$ (~2 mV), $Na_V1.6$ (~3 mV), and Na_V1.8 (\sim 2 mV). The shift in V_{1/2} for channel availability differed for Na_V1.1 (\sim 4 mV), Na_V1.6 (\sim 6 mV), and Na_V1.8 (\sim 2 mV). For all tested Na_V channel subtypes, no significant impact of GrTX-SIA was observed on recovery from the inactivation parameter (Fig. 1).

The effect of GrTX-SIA on Na_V1.6 gating parameters

Of all tested channels, Na_V1.6 was most susceptible to GrTX-SIA. We therefore focused on the next set of experiments in this subtype. When incubating Na_V1.6 with 1 μM GrTX-SIA and depolarizing the membrane to −10 mV for 50 ms at 5 s intervals up to 4 min (Fig. 2), currents were reduced by $82 \pm 7\%$ (n = 6). At 1-s intervals, current inhibition was $65 \pm 7\%$ (n = 4). When the interval was increased to 30 s (n = 6), 1 min (n = 5), 2 min (n = 6), and 4 min (n = 5), inhibition decreased to 58 ± 5%, 47 ± 8%, 39 ± 5%, and 25 ± 3%, indicating that GrTX-SIA binding can occur, at least in part, when the channel resides in the closed state. The $V_{1/2}$ for both the G-V and channel availability curve moved significantly when adding 1 μ M GrTX-SIA for 4 min (-22 ± 1 mV and -64 ± 2 mV, respectively) when compared with control recordings (-27 \pm 1 mV and -59 \pm 1 mV, respectively) (Fig. 2 and Table S2). No differences in curve slopes were noted. As with 100 nM (Fig. 1 and Fig. S1 B), 1 µM GrTX-SIA did not affect Na_V1.6 inactivation rate or recovery from fast inactivation (Fig. 2). A fit with the Hill equation of current inhibition measured at -10 mV versus different GrTX-SIA concentrations (Fig. 2 and Table S2) yielded an estimated apparent affinity value of 198 \pm 78 nM. The Hill slope of 0.82 \pm 0.21 suggested one toxin binding site, or perhaps multiple binding sites that are non- or negatively cooperative. To test whether GrTX-SIA interferes



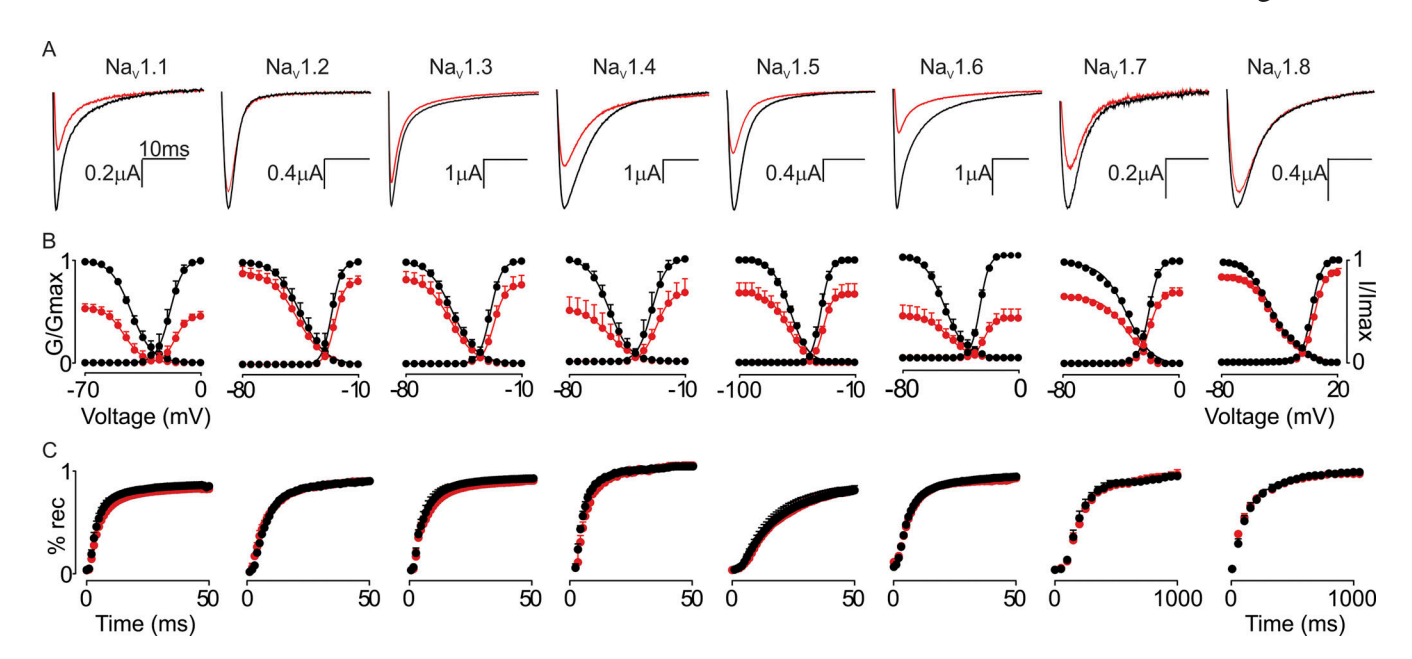


Figure 1. **GrTX-SIA inhibits multiple Na_V channel subtypes. (A–C)** Representative current traces (A), normalized conductance (G/G_{max}) -voltage and channel availability (I/I_{max}) relationships (B), and recovery from inactivation (% rec) are shown before (black) and after (red) a 4-min incubation period with 100 nM GrTX-SIA (C). Data were normalized by comparing the saturated toxin effect to the corresponding control recordings obtained before toxin addition to the same oocyte. The holding potential was -90 mV with 5 s between depolarizing pulses, except for Na_V1.8, which was measured with 10 s between pulses (protocol shown in Fig. S1). Traces shown were recorded at -15 mV for Na_V1.1, Na_V1.3, Na_V1.4, and Na_V1.7, -20 mV for Na_V1.2 and Na_V1.6, -30 mV for Na_V1.5, and +10 mV for Na_V1.8. X-axis represents 10 ms for all traces, Y-axis value is indicated. Fit values are reported in Table S1. Circles represent mean \pm SEM of n = 6 oocytes for Na_V1.1, Na_V1.5, Na_V1.6, Na_V1.7, and Na_V1.8, n = 5 oocytes for Na_V1.2 and Na_V1.4, and n = 4 oocytes for Na_V1.3.

with channel slow inactivation, we held the membrane at a range of potentials for 10 s and monitored the voltage-dependence and entry into the slow inactivated state. We noted that 1 μ M GrTX-SIA significantly shifted the V_{1/2} to hyperpolarized potentials without affecting the slope of the voltage-dependence curve (control: -25 ± 2 mV versus toxin: -49 ±7 mV). Entry into the slow-inactivated state was unaffected (Fig. S2).

While conducting these experiments, toxin application appeared to induce a biphasic inhibition of $Na_V1.6$ currents (Fig. 3, A and B). Although we observed substantial variability between

oocytes, the first phase happened rather quickly (average rate constant of 1.4 \pm 0.1 min) and was responsible for the current reduction of ~50% observed in the first 2 min after toxin application. At this time point, the $V_{1/2}$ of the G-V and channel availability curve was shifted from ~26 \pm 1 mV to ~22 \pm 1 mV and from ~54 \pm 1 mV to ~60 \pm 2 mV, respectively (Fig. 3 C). Although a clear distinction was challenging to consistently observe, a second, somewhat slower phase (average rate constant of 3.8 \pm 0.7 min) followed and increased channel inhibition further at which point the $V_{1/2}$ value of the G-V curve no longer differed from control. Total current inhibition achieved after a 4-min

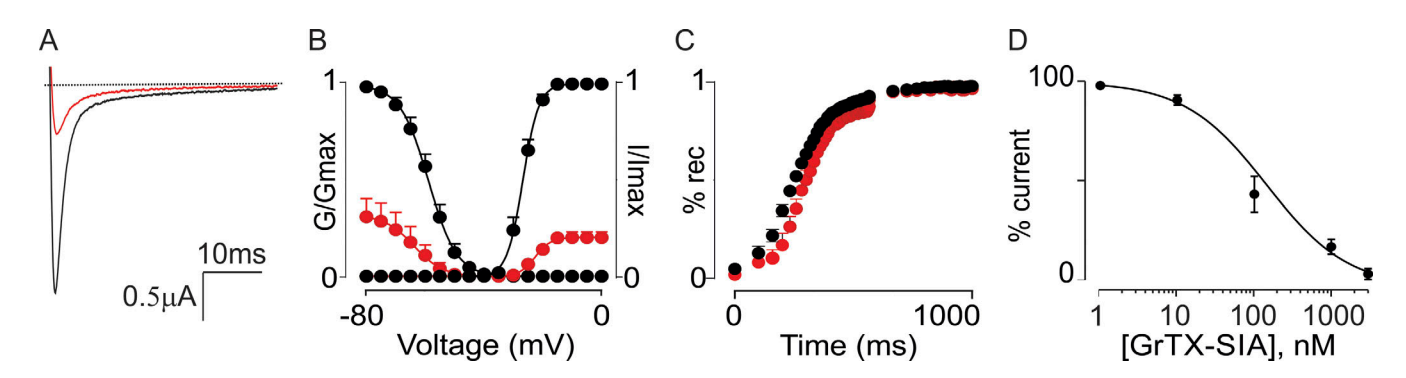


Figure 2. **GrTX-SIA inhibits Na_V1.6. (A–C)** Representative current trace recorded at -20 mV (A), normalized conductance (G/G_{max})-voltage and channel availability (I/I_{max}) relationships (B), and recovery from inactivation (% rec; C) are shown before (black) and after (red) a 4-min incubation period with 1 μ M GrTX-SIA. The holding potential was -90 mV with 5 s between depolarizing pulses (see Fig. S1). **(D)** Dose-response relationship, fitted with the Hill equation, of GrTX-SIA (concentration in nM) versus percentage of current remaining when measured at -10 mV. Circles represent mean \pm SEM of n=6 oocytes for 1 nM, 10 nM, 100 nM, and 1 μ M, and n=5 oocytes for 3 μ M.



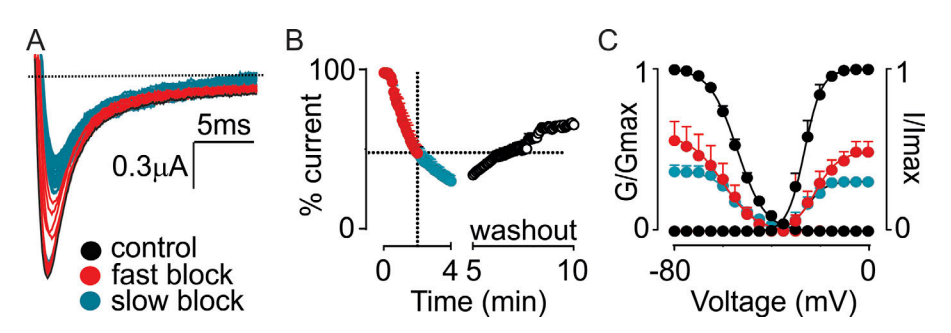


Figure 3. **GrTX-SIA inhibition of Na_V1.6 currents.** GrTX-SIA application (1 μ M) leads to a quick initial inhibition (red traces) followed by a somewhat slower and smaller inhibitory step (grey/blue). This effect was variable between measurements and only served as a rationale to investigate the potential presence of multiple toxin binding sites within Na_V1.6. **(A and B)** Panel A shows a representative trace, whereas panel B displays a typical Na_V1.6 current that is inhibited (Y-axis: percentage of current remaining assessed with 5 s pulses to -25 mV) in two

phases during a 4-min application of $1 \mu M$ GrTX-SIA. The second phase is not related to channel current rundown. Current amplitude partially recovered during a 5-min wash-off period (black circles in B). **(c)** The normalized G-V (G/G_{max}) and channel availability (I/I_{max}) relationships are shown for the starting condition without toxin (black), after the first inhibitory phase (red) and after the remaining slow step (grey/blue). Currents were recorded by applying a depolarizing voltage-step protocol from -100 to +20 mV from a holding potential of -90 mV with 5 s between depolarizing pulses. Circles represent the mean \pm SEM with n=6 oocytes.

application of 1 μM GrTX-SIA was slowly reversible and incomplete after 6 min washing with ND-100 solution (Fig. 3 B). The 4- and 6-min timescales for these experiments were chosen as a compromise between the onset of GrTX-SIA effect saturation, oocyte viability during prolonged trials, and variable start of partial Na_V1.6 current rundown observed in some oocyte batches. Combined, these data provided a motivation to check for multiple GrTX-SIA binding sites within Na_V1.6.

GrTX-SIA can interact with voltage-sensing domains II and IV in $Na_{v}1.6$

To explore whether GrTX-SIA interacts with one or more VSDs in Na_V1.6, we used K_V2.1/Na_V1.6 chimeric constructs in which known toxin-binding S3-S4 regions from each of the four voltage-sensor domains (VSDI-IV) of Na_V1.6 were transplanted into homotetrameric $K_V2.1$ channels (Montnach et al., 2022). Notably, a previous study on GrTX-SIA interactions with Na_V1.9 VSDs using this approach suggested potential binding to VSDIII and VSDIV (Bosmans et al., 2011). Additionally, it was demonstrated here that K_v2.1 channels are mildly inhibited by 500 nM GrTX-SIA. This inhibition was abolished when the S3-S4 region of VSDI or VSDII from Na_v1.9 was inserted, indicating that GrTX-SIA can also bind-with low affinity-to K_V2.1 VSDs (Bosmans et al., 2011). When applying 1 µM GrTX-SIA to the K_V2.1/Na_V1.6 chimeric constructs (Fig. 4), we observed that neither the VSDI nor the VSDIII construct was affected. In contrast, the toxin significantly inhibited K+ currents mediated by the VSDII and VSDIV chimeras indicating binding to the transferred Na_v1.6 regions. These measurements revealed distinct characteristics of GrTX-SIA interaction with VSDII and VSDIV. First, the VSDII chimera was inhibited by 67 ± 17% whereas the VSDIV construct showed a 92 ± 5% current reduction when measured at $V_{1/2}$ of the G-V curve after exposure to 1 μM toxin (Fig. 4). A fit with the Hill equation assuming occupancy of all four binding sites (Bosmans et al., 2008), yielded an apparent affinity value (Kd) of 3.1 µM for VSDII and 1.1 µM for VSDIV. Second, onset of inhibition was slower for VSDII (~4 min) compared with the VSDIV chimera (<2 min). Third, effect reversibility was much faster for VSDII with complete recovery after 4 min whereas currents of the VSDIV chimera did not yet fully recover after 10 min of washing with 50K solution (Fig. 4 B

and Fig. S3). These data suggest a preferential and tight binding to VSDIV with a secondary, lower affinity target in VSDII of $Na_{
m V}1.6$.

Next, we used AlphaFold-guided molecular modeling to predict interactions of GrTX-SIA with VSDII and VSDIV of Na_V1.6. Initial predictions with the full-length human Na_V1.6 sequence yielded nonsensical results, with GrTX-SIA either not forming contacts, or the binding site being in the toxininaccessible intracellular region. We therefore focused on predictions with the isolated VSDII and VSDIV regions. For VSDIV, the top hits all show GrTX-SIA bound to the extracellular region. Glu¹⁵⁵¹, a negatively charged residue in transmembrane segment 1 (S1), and Glu¹⁶⁰⁷ in S3 are expected to form salt bridge interactions with Lys²⁴ in GrTX-SIA (Fig. 5). For VSDII predictions, the top five hits were nonsensical, with GrTX-SIA again bound to the intracellular region. For lower-ranked hits, multiple models show GrTX-SIA interactions with the extracellular side of VSDII with residues Glu782 and Glu838 being potentially involved in GrTX-SIA binding (Fig. 5). Since the associated PAE scores are modest (\sim 20) for the VSDIV data, and the potential for ambiguity in these models, we next mutated these residues in Na_v1.6 and experimentally reassessed GrTX-SIA binding.

Na_V1.6 has at least two GrTX-SIA binding sites

Given the extensively documented binding of peptide toxins to the S3-S4 region in Na_V channel VSDs (Ahern et al., 2016) and the more pronounced binding of GrTX-SIA to the K_V2.1/Na_V1.6 VSDIV chimera, we first mutated Glu¹⁶⁰⁷ in S3 of VSDIV to a lysine (i.e., p.E1607K, VSDIVmut). This mutation resulted in a depolarizing shift of the G-V and channel availability curve by \sim 7 and \sim 17 mV, respectively (Fig. 6 and Table S3). When applying 1 µM GrTX-SIA to this mutant, we noted a substantial reduction of inhibition from ~80% with the wild-type channel to $32 \pm 1\%$ in Na_V1.6^{p.E1607K}, measured at 0 mV. Initial inhibition of current was rapid, perhaps because the p.E1607K substitution does not completely disrupt the VSDIV toxin binding site (Fig. 4). This was followed by a slower phase with an average rate constant of 6.8 ± 2.6 min (Fig. 6), likely reflecting toxin binding to VSDII (Fig. 4). No toxin-induced shift in the G-V relationship was detected, as in control conditions. Notably, the application of 1 μM GrTX-SIA to $Na_V 1.6^{p,E1607K}$ resulted in a



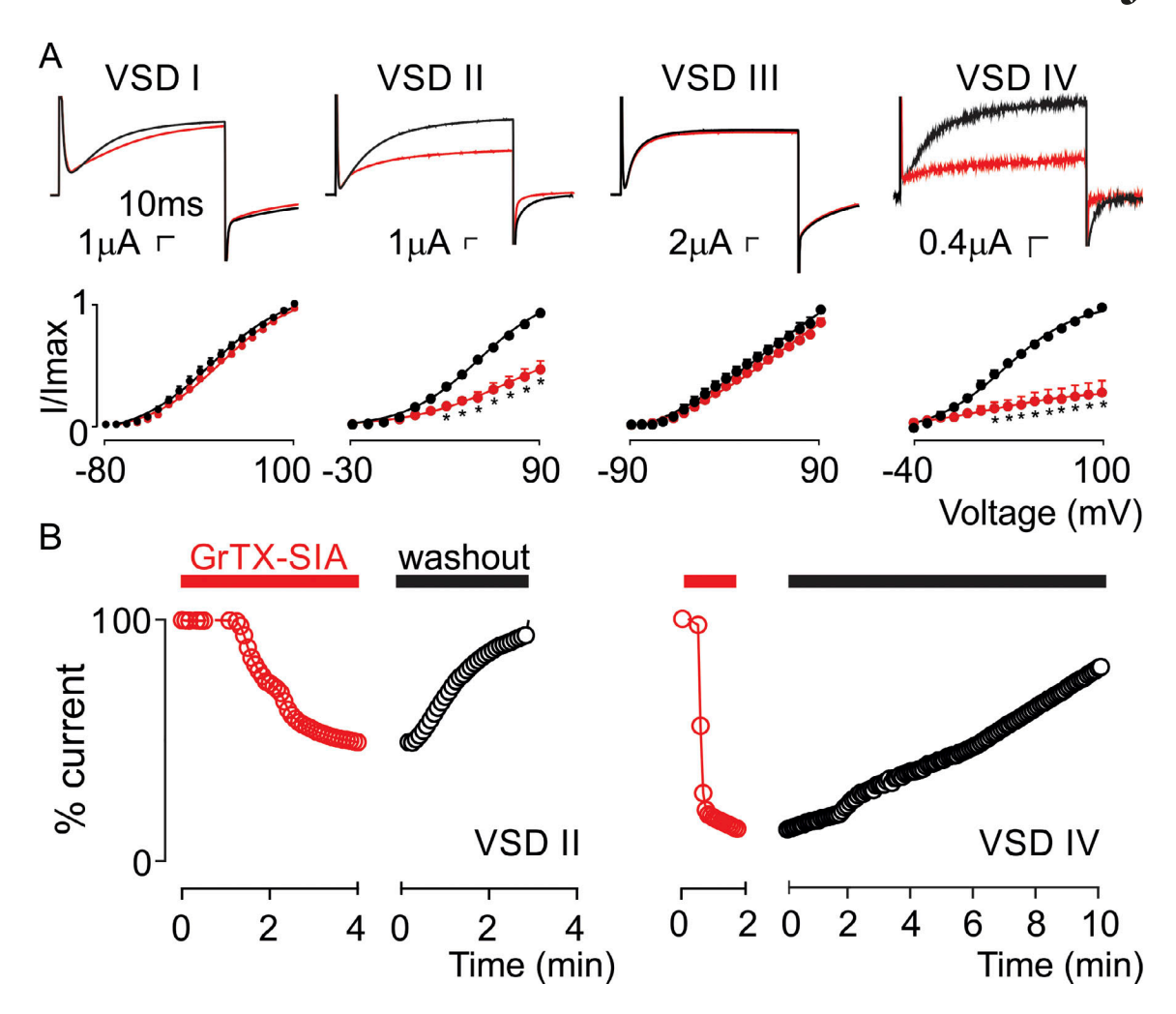


Figure 4. **GrTX-SIA interacts with two K_V2.1/Na_V1.6 VSD chimeras. (A)** Example potassium ion currents (top row) elicited by depolarizations to the maximum voltage of the voltage-activation curve (second row) for the four K_V2.1/Na_V1.6 VSD chimeras (VSDI-VSDIV) in the absence (black) and presence of 1 μ M GrTX-SIA after a 4-min incubation period. The holding voltage was -90 mV and the tail voltage was -60 mV (-80 mV for DIII). The second row of panel A shows the normalized current-voltage relationships for the corresponding K_V2.1/Na_V1.6 VSD chimeras before and after the addition of 1 μ M GrTX-SIA, normalized to the maximal control current. *P < 0.05 compared with recordings before toxin addition. **(B)** Representative example of partial K_V2.1/Na_V1.6 VSDII inhibition (left) by 1 μ M GrTX-SIA followed by wash-off with ND-100 (Y-axis: percentage of current remaining assessed with 5 s pulses to +50 mV). Current amplitude completely recovered during a 4-min wash-off period (black circles). Right panel shows virtually complete K_V2.1/Na_V1.6 VSDIV inhibition by 1 μ M GrTX-SIA followed by incomplete wash-off with ND-100 after 10 min. Data shown are mean ± SEM of n = 7 oocytes for K_V2.1/Na_V1.6 VSDI, and n = 5 oocytes for K_V2.1/Na_V1.6 VSDIV.

reduced hyperpolarizing shift in channel availability (~4 mV) compared with the wild-type channel (~9 mV). Next, we mutated Glu⁷⁸² and Glu⁸³⁸ in Na_V1.6 VSDII to lysines (i.e., p.E782K and p.E838K, VSDIImut). This double mutation resulted in a depolarizing shift of the G-V and channel availability curve by \sim 12 and \sim 3 mV, respectively (Fig. 6 and Table S3). When applying 1 µM GrTX-SIA to this mutant, we noted a large reduction of current inhibition from ~80% with the wild-type channel to $26 \pm 5\%$ in Na_V1.6 VSDII^{mut}, measured at 0 mV. The time course of inhibition displayed one phase with an average rate constant of 2.3 ± 0.2 min (Fig. 6), presumably reflecting VSDIV binding. Application of 1 µM GrTX-SIA induced a significant depolarizing shift of the G-V curve by ~3 mV whereas channel availability was unaffected (Table S3). It is worth noting here that the biphasic manner in which current inhibition in response to toxin application seemed to occur in the wild-type channel (Fig. 3) is partly reflected in the $Na_V1.6$ VSDII^{mut} (fast) and VSDIV^{mut} (slow) rate constants of binding as well as the onset of inhibition and wash-off times observed in the $K_V2.1/Na_V1.6$ VSDII and VSDIV chimeric constructs (Fig. 4).

Finally, we added the VSDII substitutions to Na_V1.6 p.E1607K (i.e., VSDII^{mut}–VSDIV^{mut}) and checked whether we could reduce GrTX-SIA efficacy even further. Inclusion of the three mutations resulted in a depolarizing shift of the G-V and channel availability curve by $\sim\!18$ and $\sim\!17$ mV, respectively, compared with the wild-type channel (Fig. 6 and Table S3). Application of 1 μ M toxin brought about only a 14 \pm 1% current inhibition after 4 min whereas wash-off was complete after $\sim\!2$ min. As in the wild-type channel, no toxin-induced shift in the G-V relationship was detected. In addition, the hyperpolarizing shift in channel availability, as seen in control and less pronounced in the Na_V1.6 p.E1607K channel, was no longer present. Combined, these data



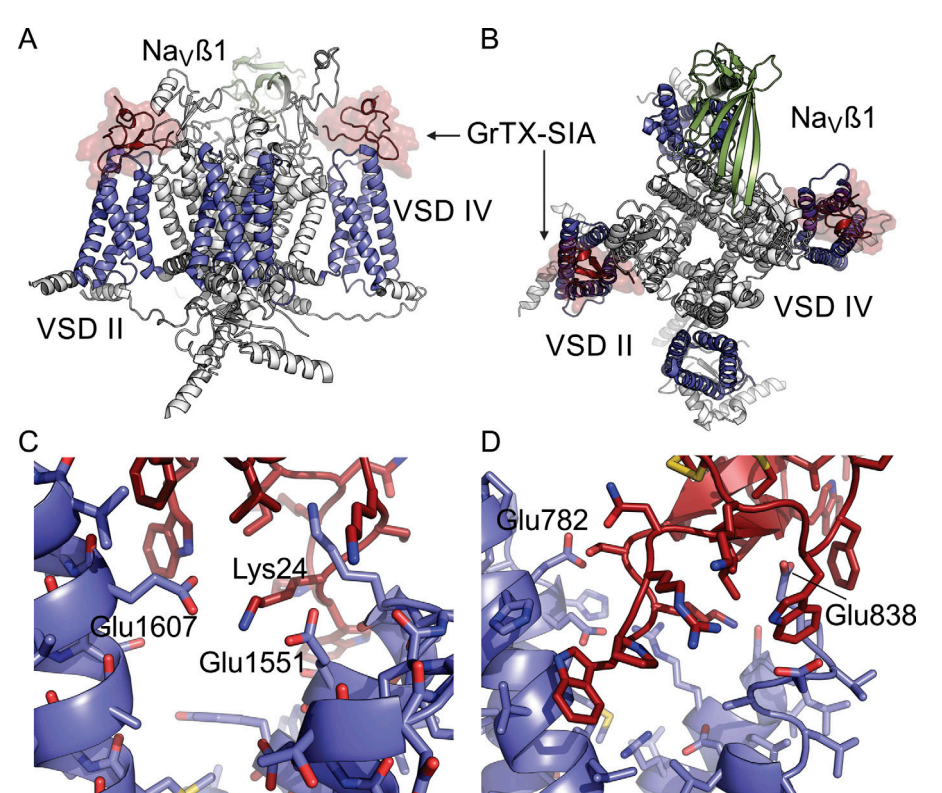


Figure 5. AlphaFold predictions for GrTX-SIA binding to human Na_V1.6. (A) Cryo-EM structure of human Na_V1.6 (PDB accession no. 8FHD) with proposed docking sites for GrTX-SIA (transparent red) on VSDII and VSDIV. Shown is a view from within the plane of the plasma membrane. The $Na_V\beta 1$ subunit is shown in green. VSDs of the channel are shown in blue and the remainder in grey. GrTX-SIA binding positions are obtained by superposition of AlphaFold models for GrTX-SIA bound to VSDII and VSDIV individually. (B) Same as in panel A, but shows a top view from the extracellular space facing the plasma membrane. (C) Top AlphaFold model for GrTX-SIA (red) bound to VSDIV (blue). Select residues are labeled. (D) AlphaFold model for GrTX-SIA (red) bound to VSDII (blue). This model corresponds to #6 in the AlphaFold model ranking, but is the highest ranked model whereby GrTX-SIA is bound to the extracellular part of VSDII. Select residues are labeled.

suggest that GrTX-SIA can inhibit $\rm Na_{\rm V}1.6$ currents by interacting with VSDII and VSDIV.

Discussion

The data reported here show that GrTX-SIA can function as an inhibitory gating modifier of multiple Na_V channel subtypes, albeit with varying efficacy. When expressed in Xenopus oocytes, Na_V1.6 is the most susceptible of all tested subtypes (Na_V1.1- $Na_V 1.8$) with ~80% of the current inhibited in the presence of 1 μM (Figs. 1 and 2; and Table S1). Markedly, K_V2.1/Na_V1.6 chimeric constructs and molecular docking combined with targeted point mutations in Na_V1.6 suggested that GrTX-SIA achieves current inhibition through interaction with regions within VSDII and VSDIV, with the latter being the higher affinity binding site (Figs. 4 and 6). Among the four Na_V channel VSDs, VSDIV is unique because of its distinct role in inactivating the channel after it has opened (examples include Lacroix et al., 2013; Ahern et al., 2016; Bezanilla, 2018; Armstrong and Hollingworth, 2018; Cowgill and Chanda, 2021). As such, toxins that primarily target this region typically impede the inactivation process. However, the inactivation gate may also close before the channel reaches a conducting state (Armstrong, 2006). Mechanistic insights such as these provided a foundation for a model in which VSDIV movement occurs in two consecutive stages: (1) partial activation associated with channel opening after either VSDI-II or VSDIII activates, and (2) full activation of VSDIV after which the inactivation particle is free to obstruct the pore and prevent further ion conduction. Our results suggest that GrTX-SIA may affect the first VSDIV movement to decrease channel conductance whereas ligands

such as the scorpion toxin AaHII and others prevent full VSDIV activation resulting in fast inactivation inhibition (Gilchrist and Bosmans, 2018; Clairfeuille et al., 2019; Jiang et al., 2021). It is worth noting that GrTX-SIA efficacy is further increased by an additional binding site within VSDII (Fig. 4), a region of the channel involved in pore opening (Ahern et al., 2016).

The results of this study combined with previous work on GrTX-SIA and similar toxins underscore the notion that these ligands can recognize and bind to a conserved three-dimensional module in Ca_V channels, Na_V channels, K_V channels, and possibly other ion channel families as well (examples include Siemens et al., 2006; Ono et al., 2011; Bohlen et al., 2010; Jensen et al., 2014; Kalia et al., 2015). Indeed, an extensive body of functional and structural evidence illustrates that voltage-gated ion channels follow a multidomain architecture whereby the Ca²⁺-, Na⁺-, or K⁺-selective pore domain has diverged to confer selectivity for a particular ion whereas the separate VSDs, which are largely conserved in their structure, are shared by all of them (examples include Long et al., 2005, 2007; Payandeh et al., 2011; de Lera Ruiz and Kraus, 2015; Wu et al., 2015; Tang et al., 2016; Pan et al., 2018; Shen et al., 2019; Clairfeuille et al., 2019; Noreng et al., 2021; Catterall, 2023). It is worth mentioning here that GrTX-SIA was part of a large-scale production effort of >600 cysteine-dense peptides that were screened for activity on a subset of ion channels using a commercial electrophysiology assay platform (Correnti et al., 2018). It was noted in the supplementary materials of this publication that GrTX-SIA could inhibit particular Cav, Nav, Kv, and Transient Receptor Potential channel subtypes at 20 µM, a rather high concentration that may reflect the variability associated with high-throughput ion channel electrophysiology approaches. Alternatively, variations



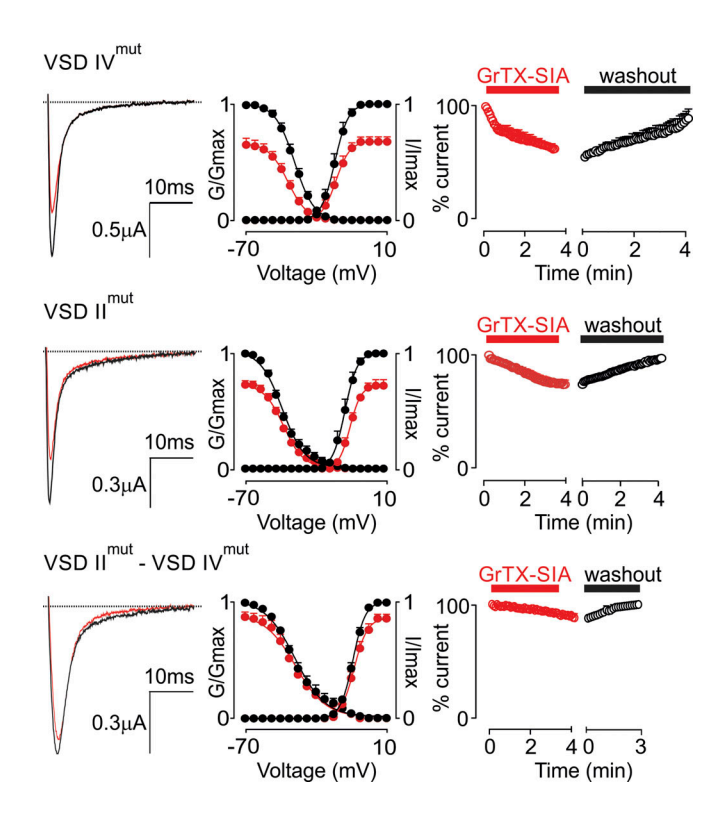


Figure 6. **Mutations in Na_V1.6 VSDII and VSDIV influence GrTX-SIA binding.** The effect of 1 μ M GrTX-SIA on Na_V1.6 VSDIV^{mut} is drastically reduced compared to the wild-type channel. The top row shows a representative trace before (black) and after (red) toxin application for 4 min, the normalized G-V (G/G_{max}) and channel availability (I/I_{max}) relationships under these conditions, and a representative example of partial Na_V1.6 VSDIV^{mut} inhibition by 1 μ M GrTX-SIA followed by complete wash-off with ND-100 after 4 min. The bottom row displays the virtual lack of effect of 1 μ M GrTX-SIA on the Na_V1.6 VSDII^{mut}-VSDIV^{mut} construct. In both panels, circles represent the mean \pm SEM of n = 8 oocytes for Na_V1.6 VSDIV^{mut} and 5 oocytes for Na_V1.6 VSDII^{mut}-VSDIV^{mut}, with n = 3 for toxin wash-in/wash-off experiments.

in toxin efficacy across different heterologous expression systems might be attributed to toxin-membrane interactions, particularly when testing peptides like GrTX-SIA that have a hydrophobic protrusion (Mihailescu et al., 2014; Takeuchi et al., 2002; Milescu et al., 2009). Combined with data reported here, this entails that although comprehensive gating-modifier peptides such as GrTX-SIA are superb tools to investigate ion channel function, their potential promiscuous nature requires a thorough characterization before robust conclusions can be drawn, in particular when used in complex systems that comprise multiple ion channel families.

Data availability

Data are available in the article itself and its supplementary materials. Additional data are available from the corresponding author upon reasonable request via email.

Acknowledgments

Jeanne M. Nerbonne served as editor.

We thank the members of the Bosmans and Van Petegem laboratories for their helpful discussions.

This work was partly funded by a research grant from the Research Foundation—Flanders under G000220N. R.d.C. Collaço is funded by an FWO junior postdoctoral fellowship under application 12Z3922N.

Author contributions: R.d.C. Collaço: Conceptualization, Data curation, Formal analysis, Funding acquisition, Investigation, Methodology, Project administration, Resources, Software, Supervision, Validation, Visualization, Writing—original draft, Writing—review & editing, F. Van Petegem: Investigation, Writing—review & editing, F. Bosmans: Conceptualization, Data curation, Formal analysis, Funding acquisition, Investigation, Methodology, Project administration, Resources, Supervision, Validation, Visualization, Writing—original draft, Writing—review & editing.

Disclosures: The authors declare no competing interests exist.

Submitted: 9 February 2024 Revised: 14 June 2024 Accepted: 10 July 2024

References

Ahern, C.A., J. Payandeh, F. Bosmans, and B. Chanda. 2016. The hitchhiker's guide to the voltage-gated sodium channel galaxy. *J. Gen. Physiol.* 147: 1–24. https://doi.org/10.1085/jgp.201511492

Armstrong, C.M. 2006. Na channel inactivation from open and closed states. *Proc. Natl. Acad. Sci. USA.* 103:17991–17996. https://doi.org/10.1073/pnas.0607603103

Armstrong, C.M., and S. Hollingworth. 2018. A perspective on Na and K channel inactivation. J. Gen. Physiol. 150:7–18. https://doi.org/10.1085/jgp.201711835

Bezanilla, F. 2018. Gating currents. J. Gen. Physiol. 150:911-932. https://doi.org/10.1085/jgp.201812090

Bladen, C., J. Hamid, I.A. Souza, and G.W. Zamponi. 2014. Block of T-type calcium channels by protoxins I and II. Mol. Brain. 7:36. https://doi.org/ 10.1186/1756-6606-7-36

Bohlen, C.J., A. Priel, S. Zhou, D. King, J. Siemens, and D. Julius. 2010. A bivalent tarantula toxin activates the capsaicin receptor, TRPVI, by targeting the outer pore domain. Cell. 141:834–845. https://doi.org/10.1016/j.cell.2010.03.052

Bosmans, F., M.-F. Martin-Eauclaire, and K.J. Swartz. 2008. Deconstructing voltage sensor function and pharmacology in sodium channels. *Nature*. 456:202–208. https://doi.org/10.1038/nature07473

Bosmans, F., M. Puopolo, M.-F. Martin-Eauclaire, B.P. Bean, and K.J. Swartz. 2011. Functional properties and toxin pharmacology of a dorsal root ganglion sodium channel viewed through its voltage sensors. J. Gen. Physiol. 138:59-72. https://doi.org/10.1085/jgp.201110614

Bosmans, F., and K.J. Swartz. 2010. Targeting voltage sensors in sodium channels with spider toxins. *Trends Pharmacol. Sci.* 31:175–182. https://doi.org/10.1016/j.tips.2009.12.007

Bourinet, E., S.C. Stotz, R.L. Spaetgens, G. Dayanithi, J. Lemos, J. Nargeot, and G.W. Zamponi. 2001. Interaction of SNX482 with domains III and IV inhibits activation gating of alpha(1E) (Ca(V)2.3) calcium channels. *Biophys. J.* 81:79-88. https://doi.org/10.1016/S0006-3495(01)75681-0

Campos, F.V., B. Chanda, P.S.L. Beirão, and F. Bezanilla. 2008. Alpha-scorpion toxin impairs a conformational change that leads to fast inactivation of muscle sodium channels. J. Gen. Physiol. 132:251–263. https://doi.org/10 .1085/jgp.200809995

Catterall, W.A. 2011. Voltage-gated calcium channels. Cold Spring Harb. Perspect. Biol. 3:a003947. https://doi.org/10.1101/cshperspect.a003947

Catterall, W.A. 2023. Voltage gated sodium and calcium channels: Discovery, structure, function, and Pharmacology. Channels. 17:2281714. https://doi.org/10.1080/19336950.2023.2281714



- Catterall, W.A., M.J. Lenaeus, and T.M. Gamal El-Din. 2020. Structure and pharmacology of voltage-gated sodium and calcium channels. *Annu. Rev. Pharmacol. Toxicol.* 60:133–154. https://doi.org/10.1146/annurev-pharmtox-010818-021757
- Chakrapani, S., L.G. Cuello, D.M. Cortes, and E. Perozo. 2008. Structural dynamics of an isolated voltage-sensor domain in a lipid bilayer. *Structure*. 16:398–409. https://doi.org/10.1016/j.str.2007.12.015
- Chanda, B., O.K. Asamoah, and F. Bezanilla. 2004. Coupling interactions between voltage sensors of the sodium channel as revealed by site-specific measurements. *J. Gen. Physiol.* 123:217–230. https://doi.org/10.1085/jgp.200308971
- Chanda, B., and F. Bezanilla. 2002. Tracking voltage-dependent conformational changes in skeletal muscle sodium channel during activation. J. Gen. Physiol. 120:629-645. https://doi.org/10.1085/jgp.20028679
- Clairfeuille, T., A. Cloake, D.T. Infield, J.P. Llongueras, C.P. Arthur, Z.R. Li, Y. Jian, M.-F. Martin-Eauclaire, P.E. Bougis, C. Ciferri, et al. 2019. Structural basis of α -scorpion toxin action on Na $_{\rm v}$ channels. *Science*. 363: eaav8573. https://doi.org/10.1126/science.aav8573
- Correnti, C.E., M.M. Gewe, C. Mehlin, A.D. Bandaranayake, W.A. Johnsen, P.B. Rupert, M.-Y. Brusniak, M. Clarke, S.E. Burke, W. De Van Der Schueren, et al. 2018. Screening, large-scale production and structure-based classification of cystine-dense peptides. *Nat. Struct. Mol. Biol.* 25: 270–278. https://doi.org/10.1038/s41594-018-0033-9
- Cowgill, J., and B. Chanda. 2021. Mapping electromechanical coupling pathways in voltage-gated ion channels: Challenges and the way forward. *J. Mol. Biol.* 433:167104. https://doi.org/10.1016/j.jmb.2021.167104
- Dongol, Y., F.C. Cardoso, and R.J. Lewis. 2019. Spider knottin pharmacology at voltage-gated sodium channels and their potential to modulate pain pathways. *Toxins*. 11:626. https://doi.org/10.3390/toxins11110626
- Gilchrist, J., and F. Bosmans. 2018. Using voltage-sensor toxins and their molecular targets to investigate Na_V 1.8 gating. J. Physiol. 596:1863–1872. https://doi.org/10.1113/JP275102
- Hodgkin, A.L., and A.F. Huxley. 1952. A quantitative description of membrane current and its application to conduction and excitation in nerve. J. Physiol. 117:500-544. https://doi.org/10.1113/jphysiol.1952.sp004764
- Jensen, J.E., B. Cristofori-Armstrong, R. Anangi, K.J. Rosengren, C.H.Y. Lau, M. Mobli, A. Brust, P.F. Alewood, G.F. King, and L.D. Rash. 2014. Understanding the molecular basis of toxin promiscuity: The analgesic sea anemone peptide APETx2 interacts with acid-sensing ion channel 3 and hERG channels via overlapping pharmacophores. J. Med. Chem. 57: 9195–9203. https://doi.org/10.1021/jm501400p
- Jiang, D., L. Tonggu, T.M. Gamal El-Din, R. Banh, R. Pomès, N. Zheng, and W.A. Catterall. 2021. Structural basis for voltage-sensor trapping of the cardiac sodium channel by a deathstalker scorpion toxin. *Nat. Commun.* 12:128. https://doi.org/10.1038/s41467-020-20078-3
- Jiang, Y., A. Lee, J. Chen, V. Ruta, M. Cadene, B.T. Chait, and R. MacKinnon. 2003. X-ray structure of a voltage-dependent K+ channel. *Nature*. 423: 33–41. https://doi.org/10.1038/nature01580
- Jumper, J., R. Evans, A. Pritzel, T. Green, M. Figurnov, O. Ronneberger, K. Tunyasuvunakool, R. Bates, A. Žídek, A. Potapenko, et al. 2021. Highly accurate protein structure prediction with AlphaFold. *Nature*. 596: 583–589. https://doi.org/10.1038/s41586-021-03819-2
- Kalia, J., M. Milescu, J. Salvatierra, J. Wagner, J.K. Klint, G.F. King, B.M. Olivera, and F. Bosmans. 2015. From foe to friend: Using animal toxins to investigate ion channel function. *J. Mol. Biol.* 427:158–175. https://doi.org/10.1016/j.jmb.2014.07.027
- Keith, R.A., T.J. Mangano, R.A. Lampe, P.A. DeFeo, M.J. Hyde, and B.A. Donzanti. 1995. Comparative actions of synthetic omega-grammotoxin SIA and synthetic omega-Aga-IVA on neuronal calcium entry and evoked release of neurotransmitters in vitro and in vivo. Neuropharmacology. 34:1515–1528. https://doi.org/10.1016/0028-3908(95)00075-h
- Kuang, Q., P. Purhonen, and H. Hebert. 2015. Structure of potassium channels. Cell. Mol. Life Sci. 72:3677–3693. https://doi.org/10.1007/s00018-015-1948-5
- Lacroix, J.J., F.V. Campos, L. Frezza, and F. Bezanilla. 2013. Molecular bases for the asynchronous activation of sodium and potassium channels required for nerve impulse generation. *Neuron*. 79:651–657. https://doi.org/10.1016/j.neuron.2013.05.036
- Lampe, R.A., P.A. Defeo, M.D. Davison, J. Young, J.L. Herman, R.C. Spreen, M.B. Horn, T.J. Mangano, and R.A. Keith. 1993. Isolation and pharmacological characterization of omega-grammotoxin SIA, a novel peptide inhibitor of neuronal voltage-sensitive calcium channel responses. Mol. Pharmacol. 44:451-460.

- de Lera Ruiz, M., and R.L. Kraus. 2015. Voltage-gated sodium channels: Structure, function, pharmacology, and clinical indications. *J. Med. Chem.* 58:7093-7118. https://doi.org/10.1021/jm501981g
- Li, Z., Q. Wu, and N. Yan. 2024. A structural atlas of druggable sites on Na_v channels. Channels. 18:2287832. https://doi.org/10.1080/19336950.2023
- Li-Smerin, Y., and K.J. Swartz. 1998. Gating modifier toxins reveal a conserved structural motif in voltage-gated Ca2+ and K+ channels. Proc. Natl. Acad. Sci. USA. 95:8585–8589. https://doi.org/10.1073/pnas.95.15.8585
- Long, S.B., E.B. Campbell, and R. Mackinnon. 2005. Crystal structure of a mammalian voltage-dependent Shaker family K+ channel. Science. 309: 897–903. https://doi.org/10.1126/science.1116269
- Long, S.B., X. Tao, E.B. Campbell, and R. MacKinnon. 2007. Atomic structure of a voltage-dependent K+ channel in a lipid membrane-like environment. Nature. 450:376–382. https://doi.org/10.1038/nature06265
- McDonough, S.I., R.A. Lampe, R.A. Keith, and B.P. Bean. 1997. Voltage-dependent inhibition of N- and P-type calcium channels by the peptide toxin omega-grammotoxin-SIA. Mol. Pharmacol. 52:1095–1104. https://doi.org/10.1124/mol.52.6.1095
- Meng, E.C., T.D. Goddard, E.F. Pettersen, G.S. Couch, Z.J. Pearson, J.H. Morris, and T.E. Ferrin. 2023. UCSF ChimeraX: Tools for structure building and analysis. Protein Sci. 32:e4792. https://doi.org/10.1002/pro.4792
- Mihailescu, M., D. Krepkiy, M. Milescu, K. Gawrisch, K.J. Swartz, and S. White. 2014. Structural interactions of a voltage sensor toxin with lipid membranes. Proc. Natl. Acad. Sci. USA. 111:E5463–E5470. https://doi.org/10.1073/pnas.1415324111
- Milescu, M., F. Bosmans, S. Lee, A.A. Alabi, J.I. Kim, and K.J. Swartz. 2009. Interactions between lipids and voltage sensor paddles detected with tarantula toxins. Nat. Struct. Mol. Biol. 16:1080–1085. https://doi.org/10.1038/nsmb.1679
- Montnach, J., L.A. Blömer, L. Lopez, L. Filipis, H. Meudal, A. Lafoux, S. Nicolas, D. Chu, C. Caumes, R. Béroud, et al. 2022. In vivo spatiotemporal control of voltage-gated ion channels by using photoactivatable peptidic toxins. *Nat. Commun.* 13:417. https://doi.org/10.1038/s41467-022-27974
- Ngo, K., D. Lopez Mateos, Y. Han, K.C. Rouen, S.-H. Ahn, H. Wulff, C.E. Clancy, V. Yarov-Yarovoy, and I. Vorobyov. 2024. Elucidating molecular mechanisms of protoxin-II state-specific binding to the human NaV1.7 channel. J. Gen. Physiol. 156:e202313368. https://doi.org/10.1085/jgp.202313368
- Noreng, S., T. Li, and J. Payandeh. 2021. Structural pharmacology of voltage-gated sodium channels. *J. Mol. Biol.* 433:166967. https://doi.org/10.1016/j.jmb.2021.166967
- Norton, R.S., and S.I. McDonough. 2008. Peptides targeting voltage-gated calcium channels. Curr. Pharm. Des. 14:2480-2491. https://doi.org/10 .2174/138161208785777478
- Ono, S., T. Kimura, and T. Kubo. 2011. Characterization of voltage-dependent calcium channel blocking peptides from the venom of the tarantula Grammostola rosea. Toxicon. 58:265-276. https://doi.org/10.1016/j .toxicon.2011.06.006
- Pallaghy, P.K., K.J. Nielsen, D.J. Craik, and R.S. Norton. 1994. A common structural motif incorporating a cystine knot and a triple-stranded betasheet in toxic and inhibitory polypeptides. *Protein Sci.* 3:1833–1839. https://doi.org/10.1002/pro.5560031022
- Pan, X., Z. Li, Q. Zhou, H. Shen, K. Wu, X. Huang, J. Chen, J. Zhang, X. Zhu, J. Lei, et al. 2018. Structure of the human voltage-gated sodium channel Na_v1.4 in complex with β1. Science. 362:eaau2486. https://doi.org/10.1126/science.aau2486
- Payandeh, J., T. Scheuer, N. Zheng, and W.A. Catterall. 2011. The crystal structure of a voltage-gated sodium channel. *Nature*. 475:353–358. https://doi.org/10.1038/nature10238
- Piser, T.M., R.A. Lampe, R.A. Keith, and S.A. Thayer. 1994. omega-Grammotoxin blocks action-potential-induced Ca2+ influx and wholecell Ca2+ current in rat dorsal-root ganglion neurons. *Pflugers Arch.* 426: 214–220. https://doi.org/10.1007/BF00374774
- Piser, T.M., R.A. Lampe, R.A. Keith, and S.A. Thayer. 1995a. Omegagrammotoxin SIA blocks multiple, voltage-gated, Ca2+ channel subtypes in cultured rat hippocampal neurons. Mol. Pharmacol. 48:131-139.
- Piser, T.M., R.A. Lampe, R.A. Keith, and S.A. Thayer. 1995b. Complete and reversible block by omega-grammotoxin SIA of glutamatergic synaptic transmission between cultured rat hippocampal neurons. Neurosci. Lett. 201:135–138. https://doi.org/10.1016/0304-3940(95)12169-2
- Sheets, M.F., J.W. Kyle, R.G. Kallen, and D.A. Hanck. 1999. The Na channel voltage sensor associated with inactivation is localized to the external



- charged residues of domain IV, S4. Biophys. J. 77:747-757. https://doi.org/10.1016/S0006-3495(99)76929-8
- Shen, H., D. Liu, K. Wu, J. Lei, and N. Yan. 2019. Structures of human $Na_v1.7$ channel in complex with auxiliary subunits and animal toxins. Science. 363:1303-1308. https://doi.org/10.1126/science.aaw2493
- Siemens, J., S. Zhou, R. Piskorowski, T. Nikai, E.A. Lumpkin, A.I. Basbaum, D. King, and D. Julius. 2006. Spider toxins activate the capsaicin receptor to produce inflammatory pain. *Nature*. 444:208–212. https://doi.org/10.1038/nature05285
- Swartz, K.J. 2008. Sensing voltage across lipid membranes. *Nature*. 456: 891–897. https://doi.org/10.1038/nature07620
- Swartz, K.J., and R. MacKinnon. 1995. An inhibitor of the Kv2.1 potassium channel isolated from the venom of a Chilean tarantula. *Neuron.* 15: 941-949. https://doi.org/10.1016/0896-6273(95)90184-1
- Swartz, K.J., and R. MacKinnon. 1997. Mapping the receptor site for hanatoxin, a gating modifier of voltage-dependent K+ channels. *Neuron.* 18: 675–682. https://doi.org/10.1016/s0896-6273(00)80307-4

- Takeuchi, K., E. Park, C. Lee, J. Kim, H. Takahashi, K. Swartz, and I. Shimada. 2002. Solution structure of omega-grammotoxin SIA, a gating modifier of P/Q and N-type Ca(2+) channel. *J. Mol. Biol.* 321:517–526. https://doi.org/10.1016/s0022-2836(02)00595-8
- Tang, L., T.M. Gamal El-Din, T.M. Swanson, D.C. Pryde, T. Scheuer, N. Zheng, and W.A. Catterall. 2016. Structural basis for inhibition of a voltage-gated Ca²⁺ channel by Ca²⁺ antagonist drugs. *Nature*. 537:117–121. https://doi.org/10.1038/nature19102
- Van Theemsche, K.M., D.V. Van de Sande, D.J. Snyders, and A.J. Labro. 2020. Hydrophobic drug/toxin binding sites in voltage-dependent K⁺ and Na⁺ channels. Front. Pharmacol. 11:735. https://doi.org/10.3389/fphar .2020.00735
- Wu, J., Z. Yan, Z. Li, C. Yan, S. Lu, M. Dong, and N. Yan. 2015. Structure of the voltage-gated calcium channel Cavl.1 complex. Science. 350:aad2395. https://doi.org/10.1126/science.aad2395
- Yao, X., S. Gao, and N. Yan. 2024. Structural biology of voltage-gated calcium channels. Channels. 18:2290807. https://doi.org/10.1080/19336950.2023 2290807



Supplemental material

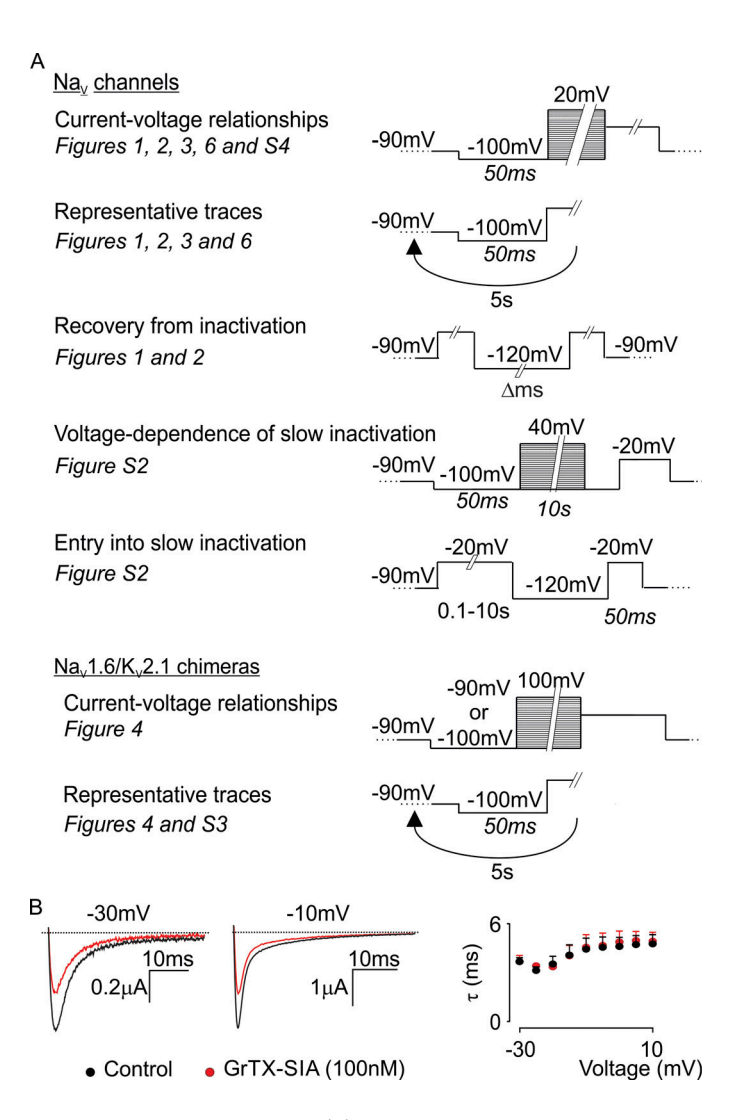


Figure S1. **Electrophysiology protocols used and Na_V1.6 inactivation. (A)** Shown are illustrations of the voltage-step protocols used in experimental work. **(B)** 100 nM GrTX-SIA does not influence the inactivation rate of Na_V1.6. Representative current traces at -30 and -10 mV are shown before (black) and after (red) a 4-min incubation period with 100 nM GrTX-SIA. A single exponential fit of the inactivation phase yielded a time constant (τ) that is plotted against its voltage step in the right panel. Circles represent mean \pm standard error of the mean (SEM) of n=6 oocytes.



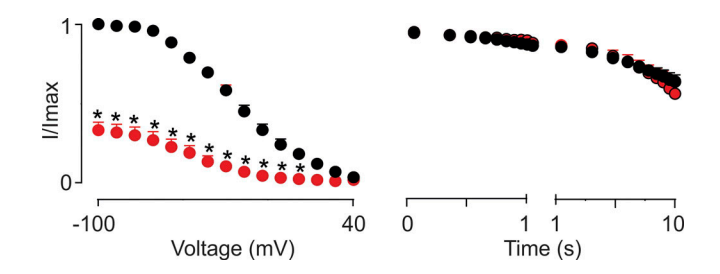


Figure S2. **GrTX-SIA and Na_V1.6 slow inactivation.** 1 μ M GrTX-SIA affects the voltage-dependence of slow inactivation (left) but not entry into slow inactivation (right). Control is shown in black and toxin condition in red. Circles represent the mean \pm SEM of n=8 oocytes for voltage-dependence of slow inactivation and n=5 oocytes for entry into slow inactivation; *P < 0.05 compared to without toxin.

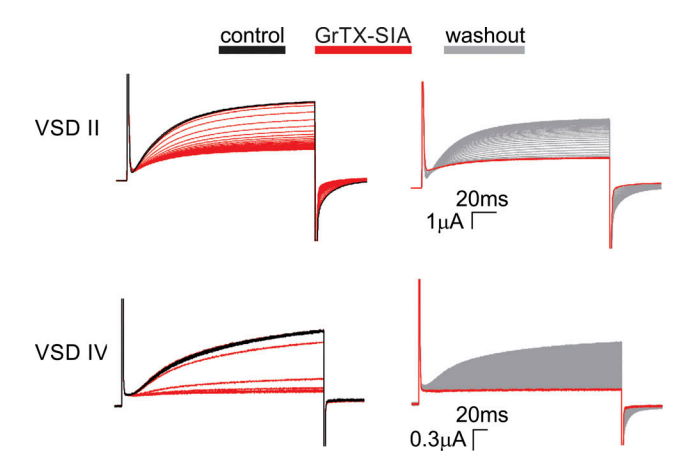


Figure S3. **GrTX-SIA interacts with VSDII and VSDIV in Na_V1.6.** Shown are representative current traces of $K_V2.1/Na_V1.6$ VSDII (top) and $K_V2.1/Na_V1.6$ VSDIV (bottom) before (black; control) and during 1 μ M GrTX-SIA application (red) for 4 min. Grey traces indicate recovery of ionic currents upon toxin washout with 50K solution. These data underscore the notion that GrTX-SIA inhibited the $K_V2.1/Na_V1.6$ VSDII chimera more slowly compared to $K_V2.1/Na_V1.6$ VSDIV. Moreover, current recovery was faster for the $K_V2.1/Na_V1.6$ VSDII chimera compared with $K_V2.1/Na_V1.6$ VSDIV.

Provided online are three tables. Table S1 shows influence of GrTX-SIA on the gating properties of $Na_V1.1-1.8$. Table S2 shows concentration-response data. Table S3 shows influence of GrTX-SIA on the gating properties of $Na_V1.6$ mutants.